Numerical study of strained InGaAs quantum well lasers emitting at 2.33 μm using the eight-band model*

Wang Ming(汪 明), Gu Yong-Xian(谷永先), Ji Hai-Ming(季海铭),
Yang Tao(杨 涛)†, and Wang Zhan-Guo(王占国)

Key Laboratory of Semiconductor Materials Science, Institute of Semiconductors, Chinese Academy of Sciences, Beijing 100083, *China*

(Received 15 December 2010; revised manuscript received 1 February 2011)

We investigate the band structure of a compressively strained In(Ga)As/$In_{0.53}Ga_{0.47}As$ quantum well (QW) on an InP substrate using the eight-band $\boldsymbol{k}\cdot\boldsymbol{p}$ theory. Aiming at the emission wavelength around 2.33 μm, we discuss the influences of temperature, strain and well width on the band structure and on the emission wavelength of the QW. The wavelength increases with the increase of temperature, strain and well width. Furthermore, we design an InAs /$In_{0.53}Ga_{0.47}As$ QW with a well width of 4.1 nm emitting at 2.33 μm by optimizing the strain and the well width.

Keywords: band structure, eight-band $\boldsymbol{k}\cdot\boldsymbol{p}$ theory, strained quantum well, peak emission wavelength

PACS: 73.21.Fg, 78.67.De, 78.20.Bh **DOI:** 10.1088/1674-1056/20/7/077301

1. Introduction

Mid-infrared lasers with AN emission wavelength beyond 2 μm have attracted considerable interest due to their potential application as light sources for trace-gas sensing.[1] To realize this, there are two types of material systems in experiment: GaSb-based materials and InP-based materials.[2−4] Unlike GaSb-based lasers, InP-based lasers, which consist of compressively strained InGaAs quantum wells (QWs) as the active regions, are more favourable for the application owing to their advantages of low cost, good thermal stability and mature fabrication process.[5−7] In 1994, the active region of the QW structure consisting of InAs wells and $In_{0.53}Ga_{0.47}As$ barriers, whose lattices were matched to the InP substrate, was first adopted in mid-IR laser research.[8] From then on, there have been a lot of reports on QW lasers with InAs quantum wells, especially on the distributed feedback (DFB) QW lasers fabricated by organometallic vapor-phase epitaxy (MOVPE) that broke through in emitting around 2.33 μm.[9,10]

Since the strains of these QWs are extremely large compared with those of conventional QWs, and the electrical and optical characteristics of these devices are strongly dependent on their band structures, an accurate and reliable theoretical model for calculating the band structure of highly strained QWs is indispensible. Especially for gas sensing applications in the mid-infrared region, the design of the emission wavelength is very important, since the environmental gas has very narrow absorption lines.

Fujisawa *et al.*[11] reported the application of an eight-band $\boldsymbol{k}\cdot\boldsymbol{p}$ model to large strained In(Ga)As quantum wells, where the eight-band model was demonstrated to be more effective than the six-band model when the strain was larger than 2%. In the present paper, we adopt the Burt–Foreman Hamiltonian, which is more exact than the symmetrized Hamiltonian,[12] to calculate the band structure of the In(Ga)As QW using the eight-band $\boldsymbol{k}\cdot\boldsymbol{p}$ model. In addition, we add the specific ingredients, such as the temperature, the strain and the well width influencing the band structure then the peak wavelengths, into the model. By optimization, it can be conducive to the experiment as regards to the In(Ga)As QW aiming at the emission wavelength of 2.33 μm.

In this paper, the eight-band $\boldsymbol{k}\cdot\boldsymbol{p}$ model with finite element method[13,14] is taken to calculate the band structure of a highly strained InGaAs QW. In Section 2.1, the eight-band $\boldsymbol{k}\cdot\boldsymbol{p}$ model is summarized. In Section 2.2, detailed analysis of the band structure of the InAs/$In_{0.53}Ga_{0.47}As$ QW is made, including changes before and after the introduction of

*Project supported by the '100 Talents Program' of Chinese Academy of Sciences, China.
†Corresponding author. E-mail: tyang@semi.ac.cn
© 2011 Chinese Physical Society and IOP Publishing Ltd

the strain. For the conduction band energy levels, a one-band model is introduced to be compared with the eight-band $\boldsymbol{k}\cdot\boldsymbol{p}$ model. In Section 3, experimental factors, such as temperature, strain and the well width influencing the peak emission wavelength are discussed.

2. Theory and calculation

2.1. Eight-band $\boldsymbol{k}\cdot\boldsymbol{p}$ theory

According to Kane's theory, we use the following set of basis:

$$(|S\uparrow\rangle,|X\uparrow\rangle,|Y\uparrow\rangle,|Z\uparrow\rangle,|S\downarrow\rangle,|X\downarrow\rangle,|Y\downarrow\rangle,|Z\downarrow\rangle)^{\mathrm{T}}, \quad (1)$$

and take the Hamiltonian in the following block matrix form:[15,16]

$$\boldsymbol{H}=\begin{pmatrix}\boldsymbol{G}(\boldsymbol{K}) & \boldsymbol{\Gamma}\\ -\bar{\boldsymbol{\Gamma}} & \bar{\boldsymbol{G}}(\boldsymbol{K})\end{pmatrix}, \quad (2)$$

where $\boldsymbol{G}$ and $\boldsymbol{\Gamma}$ are both 4×4 matrices, the former is composed of four parts $\boldsymbol{G}=\boldsymbol{G}_1+\boldsymbol{G}_2+\boldsymbol{G}_{\mathrm{so}}+\boldsymbol{G}_{\mathrm{st}}$, in which $\boldsymbol{G}_1$, $\boldsymbol{G}_2$ and $\boldsymbol{G}_{\mathrm{st}}$ denote the potential energy, the kinetic energy and the strain dependent energy, respectively, $\boldsymbol{G}_{\mathrm{so}}$ and $\boldsymbol{\Gamma}$ describe the spin orbit splitting. The four parts can be found in Appendix A. The overline denotes the complex conjugation.

Here, we consider QWs growing on a (001) InP substrate along direction z. The bulk 8×8 matrix can be converted into eight coupled differential equations by replacing k_z with $-\mathrm{i}(\partial/\partial z)$, and the equations are discretized using the finite element scheme. When Eq. (2) is applied to the hetero-structure, an incorrect symmetrized Hamiltonian was adopted in most papers. The symmetrized procedure is described as[16]

$$\begin{aligned}&Qk_i\rightarrow\left(Q\hat{k}_i+\hat{k}_iQ\right)/2,\\ &Qk_ik_j\rightarrow\left(\hat{k}_iQ\hat{k}_j+\hat{k}_jQ\hat{k}_i\right)/2,\quad i,j=x,y,z,\end{aligned}$$

where Q denotes a Kane parameter.

According to Foreman[17] and Burt's theory,[18] an unsymmetrized Hamiltonian can be obtained by using a more sophisticated replacement. In Eq. (A4), the diagonal terms are still treated in the symmetrized procedure $Qk_i^2\rightarrow\hat{k}_iQ\hat{k}_i$, while the upper triangular matrix element is treated as

$$N'k_ik_j\rightarrow\hat{k}_iN_+\hat{k}_j+\hat{k}_jN_-\hat{k}_i,$$

and the lower triangular matrix element is treated as

$$N'k_ik_j\rightarrow\hat{k}_jN_+\hat{k}_i+\hat{k}_iN_-\hat{k}_j,$$

where $N_-=M-\hbar^2/2m_0$ and $N_+=N'-N_-$. N and M are Kane parameters. In Eq. (A5), the upper triangular matrix element is treated as

$$\mathrm{i}Pk_i-\mathrm{i}P\varepsilon_{ij}k_j\rightarrow\mathrm{i}P\hat{k}_i-\mathrm{i}P\varepsilon_{ij}\hat{k}_j,$$

while the lower triangular matrix element is treated as

$$-\mathrm{i}Pk_i+\mathrm{i}P\varepsilon_{ij}k_j\rightarrow-\mathrm{i}\hat{k}_iP+\mathrm{i}\hat{k}_jP\varepsilon_{ij},$$

where P denotes a Kane parameter. It is proved that spurious solutions can be effectively eliminated this way, and the parameters are all cited from Ref. [19].

Within the envelop function approximation, we have

$$H\Psi(z)=E\Psi(z), \quad (3)$$

with the envelop function and the real wave-function given by

$$\varphi(z)=\sum_{i=1}^{8}|u_i(z)|^2, \quad (4)$$

$$\begin{aligned}\Psi(z)=&\,u_1|S\uparrow\rangle+u_2|X\uparrow\rangle+u_3|Y\uparrow\rangle\\ &+u_4|Z\uparrow\rangle+u_5|S\downarrow\rangle+u_6|X\downarrow\rangle\\ &+u_7|Y\downarrow\rangle+u_8|Z\downarrow\rangle,\end{aligned} \quad (5)$$

respectively.

2.2. Calculation of band structure

We study the band structure of a compressively strained InAs/$\mathrm{In_{0.53}Ga_{0.47}As}$ QW by using the eight-band $\boldsymbol{k}\cdot\boldsymbol{p}$ model. The conduction and the valance band edges both shift due to the compressive strain caused by the lattice mismatch between the InAs well and the InP substrate.[20,21] Under the condition of compressive strain, the heavy hole (HH) and light hole (LH) valence bands are no longer degenerate around Γ. The conduction and the valence band edges shift in the following way.[20] Due to the hydrostatics deformation potential $\delta E_{\mathrm{c}}=a_{\mathrm{c}}(\varepsilon_{xx}+\varepsilon_{yy}+\varepsilon_{zz})$, where ε denotes the strain in the well and the subscripts denote the directions in the lattice, the conduction band edge shifts up to a higher level. The situation in the valence band edge is more complicated: due to the hydrostatics deformation component $\delta E_{\mathrm{v}}=a_{\mathrm{v}}(\varepsilon_{xx}+\varepsilon_{yy}+\varepsilon_{zz})$, the HH and the LH valence bands are no longer degenerate. Furthermore, because of the shear deformation component

$$\eta=-\frac{1}{2}\delta E_{\mathrm{sh}}=\frac{b}{2}(\varepsilon_{xx}+\varepsilon_{yy}-2\varepsilon_{zz}),$$

with the compressive strain, the LH band edge shifts $-\eta$, which means down to a lower level, while the HH band edge shifts up η to a higher level, which is thereafter the new valence band edge. The parameters used in the above equations are shown in Table 1.

Table 1. The parameters used in this paper. All data used for the calculation of the band structures are cited from Ref. [19]. The temperature is set to 300 K except for a_v, which is defined positive in the model following the coordinates. In the InAs/$In_{0.53}Ga_{0.47}As$ QW, the strain $\varepsilon = \varepsilon_{xx} = \varepsilon_{yy} = 3.2\%$, $\varepsilon_{zz} = -2(C_{12}/C_{11})\varepsilon$.

Parameters	InAs	GaAs	$In_xGa_{1-x}As$
a_0/Å	6.0583	5.65325	Linear interpolation
E_g/eV	0.354	1.424	$1.424 - 1.547x + 0.477x^2$
a_v/eV	1.0	1.16	Linear interpolation
a_c/eV	–5.08	–7.17	Linear interpolation
b/eV	–1.8	–2.0	Linear interpolation
C_{11}/Gpa	832.9	1221	Linear interpolation
C_{12}/Gpa	452.6	566	Linear interpolation
m_e/m_0	0.025	0.067	$0.067 - 0.051x + 0.009x^2$

We can see in Fig. 1 that in the InAs/$In_{0.53}Ga_{0.47}As$ QW, the conduction band edge shifts up to a higher level. Although the situation in the valence band edge is more complicated, the valence band edge shifts up eventually.

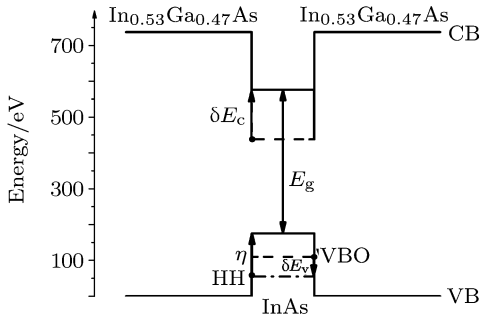


Fig. 1. Schematic diagram of energy bands in real space for a compressively strained QW structure consisting of a 5 nm InAs well sandwiched between $In_{0.53}Ga_{0.47}As$ barriers lattice-matched to an InP substrate.

The numerical results, including the electron and the hole levels and wave functions in the QW, are presented in Fig. 2. As shown in Fig. 2, in the InAs/$In_{0.53}GaAs_{0.47}$ QW with 5 nm well width, the band gap between the conduction and the valence bands is modified to 0.411 eV, which is in excellent agreement with that given in Ref. [10]. However, the conduction band offset ΔE_c is 0.148 eV, which is almost only one half of those given in Refs. [8] and [10]. To compare the energy levels in the conduction band calculated by the eight-band model, we employ a one-band model (see Appendix B), in which ΔE_c is treated as a potential barrier in the QW. The numerical result of the ground energy in the well is 580 meV in the one-band model, which is very close to E_1 of 566 meV in the eight-band model. The difference between the two models can be explained as follows: the interaction between the conduction and the valence bands is taken into consideration in the eight-band model because of the bigger effective mass and the lower energy levels in the conduction band compared with those in the one-band model, where no such interaction is considered. As we know, the parameter E_p characterizes the interaction between the conduction and the valence bands. So if $E_p \to 0$,[22] the conduction and the valence bands decouple and the eight-band model is transformed into a six-band model consisting of HH, LH and SO with the conduction band as a one-band model. In this way the interaction between the conduction and the valence bands is eliminated and E_1 is calculated to be 580 meV, which accords perfectly with that in the one-band model, as shown in Table 2.

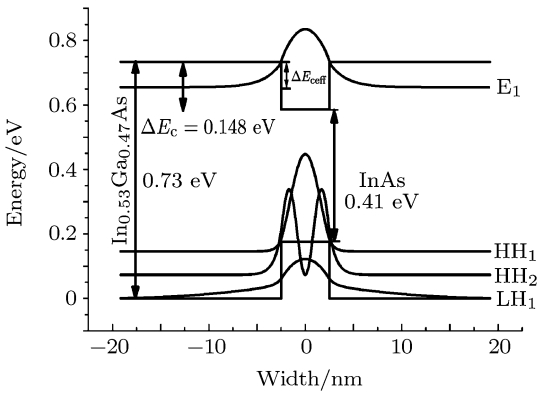


Fig. 2. Outlet of wave function of each energy sub-band and the band offsets in the InAs/$In_{0.53}Ga_{0.47}As$ QW with 5 nm well width in compressive strain. There are four bound energy levels, of which three are in the valance band and one is in the conduction band because of the quantum size effect.

Table 2. Results of energy level E_1 calculated by different models. The eight-band model with $E_p \to 0$ is transformed into a six-band model with the conduction band as a one band model.

Model	One-band	Eight-band	Eight-band^s
E_1/meV	580	566	580

3. Results and discussion

3.1. Influence of strain

For a QW consisting of a compressively strained $In_xGa_{1-x}As$ well on an InP substrate, the relationship

between the strain due to the lattice mismatch and the peak wavelength is investigated in this section. The band gap of the ternary compound $In_xGa_{1-x}As$ E_g follows Vegard's law: $E_g = 1.424 - 1.547x + 0.477x^2$. As shown in Fig. 3, the line with squares refers to the band gap of the $In_xGa_{1-x}As$ bulk without considering the strain. The band gap decreases with the indium composition increasing. When it is in the quantum well and the effect of the strain is taken into consideration (see the line with circles in Fig. 3), the band gap E_g is enlarged slightly because of the shifts of the conduction and the valence bands described in Section 2.2. Nevertheless on the whole, E_g decreases, because the band shifts caused by the strain are too small to compensate for the band gap narrowing caused by the increase of the indium composition. In the 5 nm InAs well, the energy gap between E_1 and HH_1 is mainly determined by band gap E_g. So the energy gap decreases and the peak wavelength increases with the increase of the strain eventually.

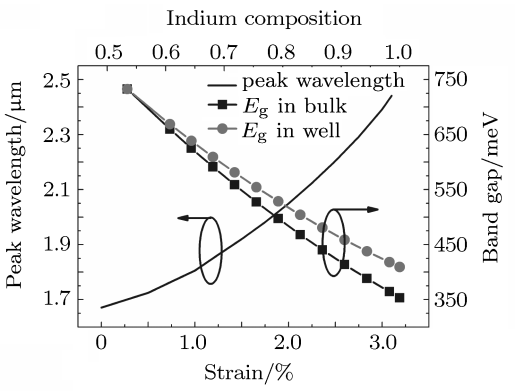


Fig. 3. Peak wavelengths and band gaps each as a function of the strain or the index of the InAs in the In(Ga)As/InGaAs QW with 5 nm well width at room temperature (300 K).

3.2. Influence of temperature

Besides the strain, the temperature is taken into consideration in the $\boldsymbol{k} \cdot \boldsymbol{p}$ model. According to Varnish's law, $E_g(T) = E_g(0)$–$\alpha T^2/(T+\beta)$, the band gap E_g should be modified with the corresponding parameters in Table 3. The dependence is approximately linear in Fig. 4(a). So we fit it linearly around the room temperature as shown in Fig. 4(b). The temperature coefficient with respect to wavelength in the QW is found to be 1.38 nm/°C, which is in excellent agreement with the experimental result of 1.40 nm/°C given in Ref. [9]. This coincides with the conclusion that the emission wavelength of the Fabry–Perot laser follows the temperature dependence of the energy gap.[23,24] Moreover, as marked with dashed line in Fig. 4(b), the temperature coefficient of the InAs bulk material is estimated to be 4.2 nm/°C. It can be deduced that with the increase of the well width, the temperature stability of the material becomes worse.

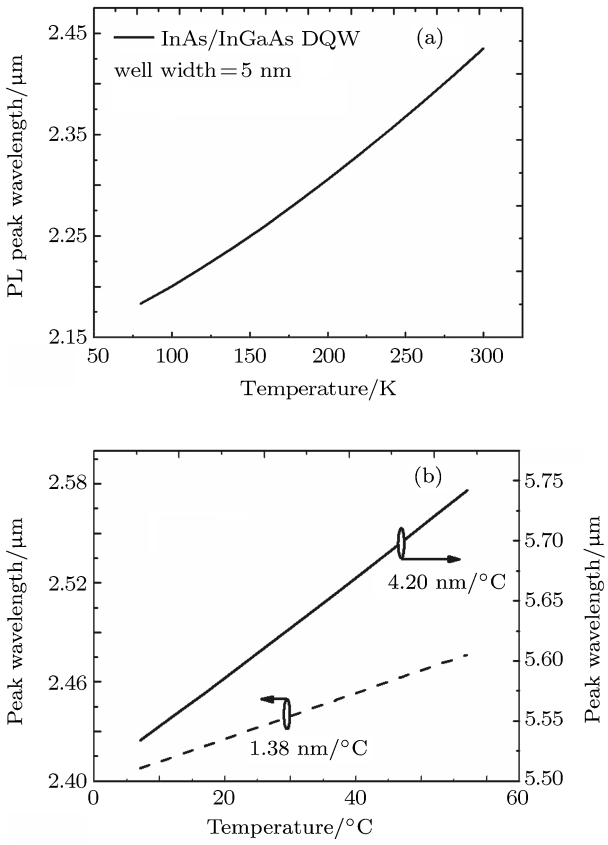


Fig. 4. (a) PL peak wavelength as a function of temperature in an InAs (5 nm)/InGaAs QW and (b) the situation around room temperature.

Table 3. Parameters used in the Varnish equation.

Parameters	InAs	GaAs
$E_g(0)$/eV	0.417	1.519
α/meV·K^{-1}	0.276	0.5405
β/K	93	204

3.3. Influence of well width

As shown in Fig. 5, the energy levels of the ground state of the electron (E_1), the ground state of the heavy hole (HH_1) and the energy gap between them (E_1–HH_1) each is a function of the well width and the indium composition x in the In(Ga)As/$In_{0.53}Ga_{0.47}As$ QW. Due to the quantum size effect, the energy difference between E_1 and E_c, as well as that between HH_1 and E_v, decreases with the increase of the well width. So the energy gap between E_1 and HH_1 narrows as

the well width increases. For the desired wavelength of 2.33 μm, the energy gap (E_1–HH_1) is estimated to be 532 meV, as marked by the dashed line parallel to the axis of the well width in Fig. 5(c). However, in the highly compressive strained ($\varepsilon > 2\%$) well, it is not easy to grow thick layers on InP substrates.[6,25]

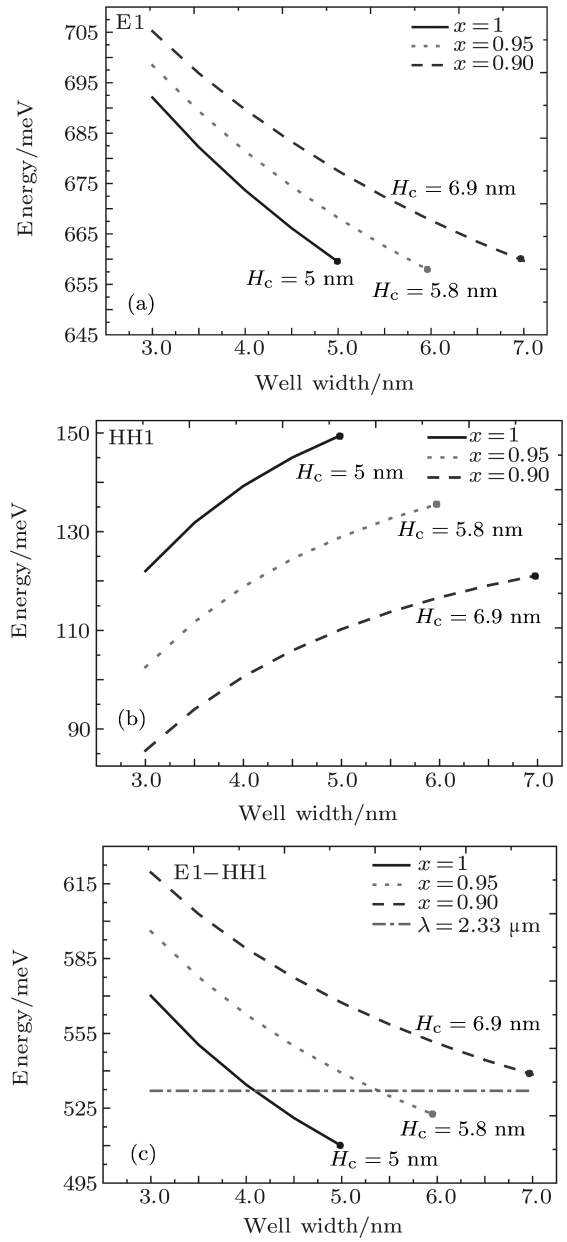


Fig. 5. (a) Curves for conduction band energy level E_1 each as a function of well width with different quantities of indium composition x; (b) curves for heavy hole band energy level HH_1 each as a function of well width with different quantities of indium composition x; (c) curves for energy gap between E_1 and HH_1 each as a function of well width with different quantities of indium composition x. The endpoint of each plot denotes the corresponding critical thickness of the wells.

On the one hand, it is the critical thickness of the well that restricts the well width. According to the Matthews–Blakeslee model[26] of the QW, the critical thickness H_c of the well is given by

$$H_c = \frac{b_1\left(1-\nu\cos^2\theta\right)}{4\pi\left(1+\nu\right)\cos\phi}\frac{1+ln\left(H_c/b_1\right)}{\varepsilon_{av}}, \tag{6}$$

with b_1 being the length of the Burgers vector, ν the Poisson ratio, ε_{av} the lattice mismatch and θ and λ the angles which define the orientation of the dislocation relative to the lattice. The calculation results for the critical thickness of the QW with indium compositions of 0.9, 0.95 and 1 are 6.9 nm, 5.8 nm and 5.0 nm, respectively, as shown by the end points in Fig. 5. In addition, even if the well width does not approach the critical thickness discussed in Section 3.2, the temperature stability of the material with a thick well is still not good. So we optimize the strain and the well width to design an InAs /$In_{0.53}Ga_{0.47}As$ QW with a well width of 4.1 nm for the emission at 2.33 μm.

4. Conclusion

We introduce an eight-band $\boldsymbol{k}\cdot\boldsymbol{p}$ model to investigate the band structure of a compressively strained InGaAs QW with an emission wavelength of 2.33 μm. We employ the eight-band $\boldsymbol{k}\cdot\boldsymbol{p}$ model to study the effects of strain, temperature and well width on the emission wavelength of the QW. The wavelength increases as the temperature, strain and well width increase. Furthermore, the numerical result of the temperature coefficient with respect to the wavelength is in good agreement with the experimental data. Aiming at the emission wavelength of 2.33 μm, we design an InAs/$In_{0.53}Ga_{0.47}As$ QW with a 4.1 nm InAs well by optimizing the strain and the well width in the strained In(Ga)As QW, which can guide the material growth and the fabrication of the corresponding lasers.

Appendix A: Eight-band $\boldsymbol{k}\cdot\boldsymbol{p}$ model

The Hamiltonian is expanded into the basis

$$\left(|S\uparrow\rangle,|X\uparrow\rangle,|Y\uparrow\rangle,|Z\uparrow\rangle,|S\downarrow\rangle,|X\downarrow\rangle,|Y\downarrow\rangle,|Z\downarrow\rangle\right)^{\mathrm{T}}, \tag{A1}$$

and takes the block matrix form

$$\boldsymbol{H} = \begin{pmatrix} \boldsymbol{G_k} & \boldsymbol{\Gamma} \\ -\bar{\boldsymbol{\Gamma}} & \bar{\boldsymbol{G}}_{\boldsymbol{k}} \end{pmatrix}, \tag{A2}$$

$$\boldsymbol{G}_1 = \begin{pmatrix} E_{\rm c} & {\rm i}Pk_x & {\rm i}Pk_y & {\rm i}Pk_z \\ -{\rm i}Pk_x & E'_{\rm v} & 0 & 0 \\ -{\rm i}Pk_y & 0 & E'_{\rm v} & 0 \\ -{\rm i}Pk_z & 0 & 0 & E'_{\rm v} \end{pmatrix}, \tag{A3}$$

$$\boldsymbol{G}_2 = \begin{pmatrix} A'K^2 & Bk_yk_z & Bk_xk_z & Bk_xk_y \\ Bk_yk_z & L'k_x^2 + M\left(k_y^2+k_z^2\right) & N'k_xk_y & N'k_xk_z \\ Bk_xk_z & N'k_yk_x & L'k_y^2 + {\rm M}\left(k_x^2+k_z^2\right) & N'k_yk_z \\ Bk_xk_y & N'k_xk_z & N'k_yk_z & L'k_z^2 + M\left(k_x^2+k_y^2\right) \end{pmatrix}, \tag{A4}$$

$$\boldsymbol{G}_{\rm st} = \begin{pmatrix} a_c\left(\varepsilon_{xx}+\varepsilon_{yy}+\varepsilon_{zz}\right) & b'\varepsilon_{yz} - {\rm i}P\varepsilon_{xj}k^j & b'\varepsilon_{zx} - {\rm i}P\varepsilon_{yj}k^j & b'\varepsilon_{xy} - {\rm i}P\varepsilon_{zj}k^j \\ b'\varepsilon_{yz} + {\rm i}P\varepsilon_{xj}k^j & l\varepsilon_{xx} + m\left(\varepsilon_{yy}+\varepsilon_{zz}\right) & n\varepsilon_{xy} & n\varepsilon_{xz} \\ b'\varepsilon_{zx} + {\rm i}P\varepsilon_{yj}k^j & n\varepsilon_{xy} & l\varepsilon_{yy} + m\left(\varepsilon_{xx}+\varepsilon_{zz}\right) & n\varepsilon_{yz} \\ b'\varepsilon_{xy} + {\rm i}P\varepsilon_{zj}k^j & n\varepsilon_{xz} & n\varepsilon_{yz} & l\varepsilon_{zz} + m\left(\varepsilon_{xx}+\varepsilon_{yy}\right) \end{pmatrix}, \tag{A5}$$

$$\boldsymbol{G}_{\rm so} = \frac{\Delta_{\rm so}}{3}\begin{pmatrix} 0 & 0 & 0 & 0 \\ 0 & 0 & -{\rm i} & 0 \\ 0 & {\rm i} & 0 & 0 \\ 0 & 0 & 0 & 0 \end{pmatrix}, \quad \boldsymbol{\Gamma} = \frac{\Delta_{\rm so}}{3}\begin{pmatrix} 0 & 0 & 0 & 0 \\ 0 & 0 & 0 & 1 \\ 0 & 0 & 0 & -{\rm i} \\ 0 & -1 & {\rm i} & 0 \end{pmatrix}, \tag{A6}$$

$$E_{\rm c} = E_{\rm v} + V_{\rm ext} + E_0, \tag{A7}$$

$$E'_{\rm v} = E_{\rm v} + V_{\rm ext} - \Delta_0/3, \tag{A8}$$

$$A' = \frac{\hbar^2}{2m_0}\left(\frac{1}{m_{\rm e}} - \frac{E_{\rm p}}{E_0}\frac{E_0 + (2\Delta_0/3)}{E_0+\Delta_0}\right), \tag{A9}$$

$$P = \sqrt{(\hbar^2/2m_0)E_{\rm p}}, \tag{A10}$$

$$L' = P^2/E_0 - (\hbar^2/2m_0)\left(\gamma_1 + 4\gamma_2\right), \tag{A11}$$

$$M = -(\hbar^2/2m_0)\left(\gamma_1 - 2\gamma_2\right), \tag{A12}$$

$$N' = P^2/E_0 - (3\hbar^2/m_0)\gamma_3, \tag{A13}$$

$$l = 2b_{\rm v} + a_{\rm c} - a_{\rm g}, \tag{A14}$$

$$m = a_{\rm c} - a_{\rm g} - b_{\rm v}, \tag{A15}$$

$$n = \sqrt{3}d_{\rm v}. \tag{A16}$$

The parameters are defined in Table A1.

Table A1. Definition of parameters used in the model.

E_0	fundamental band gap
Δ_0	spin orbit energy SO energy
$E_{\rm p}$	optical matrix parameter
$E_{\rm v}$	VB edge
$m_{\rm e}$	relative Γ-point CB mass
γ_i	Luttinger parameters (i =1, 2, 3)
B	Kane parameter
$a_{\rm c}$	hydrostatic CB deformation potential
$a_{\rm g}$	hydrostatic band gap deformation potential
$b_{\rm v}$	uniaxial ([100] direction) VB deformation potential
$d_{\rm v}$	uniaxial ([111] direction) VB deformation potential
b'	coupling the CB edge to shear strain
$V_{\rm ext}$	optional scalar potential

Appendix B: One-band model

$$U_{(x)} = \begin{cases} V_0, & |x| \geq a; \\ 0, & |x| \leq a. \end{cases} \tag{B1}$$

The Schrödinger equation in the well is

$$-\frac{\hbar^2 {\rm d}^2\varphi}{2m_1 {\rm d}x^2} = E\varphi; \tag{B2}$$

the Schrödinger equation outside the well is

$$-\frac{\hbar^2 {\rm d}^2\varphi}{2m_2 {\rm d}x^2} + V_0\varphi = E\varphi. \tag{B3}$$

Define

$$\beta^2 = \frac{2m_2\left(V_0 - E\right)}{\hbar^2}, \quad k^2 = \frac{2m_1 E}{\hbar^2}. \tag{B4}$$

According to the boundary condition, the equations are translated as follows:

$$\cos(ka) = c\,{\rm e}^{-\beta a}, \quad \frac{-k\sin(ka)}{m_1} = \frac{-\beta c\,{\rm e}^{-\beta a}}{m_2}. \tag{B5}$$

Then the solution is obtained from the following equation:

$$k^2 + \beta^2 = \frac{2\left(m_1 - m_2\right)}{\hbar^2}E + \frac{2m_2V_0}{\hbar^2}. \tag{B6}$$

Here the parameters in Eq. (B6) are assigned as follows: $m_1 = 0.025\ m_0$ and $m_2 = 0.043m_0$ according to Table 1, $E_{\rm c} = 148$ meV, $a = 2.5$ nm. We obtain the solution for Eq. (B6) $E_1 = 580$ meV.

References

[1] Choi H K 2004 *Long-Wavelength Infrared Semiconductor Lasers* (Hoboken: Wiley)

[2] Turner G W, Choi H K and Manfra M J 1998 *Appl. Phys. Lett.* **72** 876

[3] Hummer M, Rubner K, Benkert A and Forchel A 2004 *IEEE Photon. Technol. Lett.* **16** 380

[4] Gu Y, Wang K, Li Y Y, Li C and Zhang Y G 2010 *Chin. Phys.* B **19** 077304

[5] Sato T, Mitsuhara K, Watanabe T, Kasaya K, Takeshita T and Kondo Y 2007 *IEEE J. Sel. Topics Quantum Electron.* **13** 1079

[6] Sato T, Mitsuhara M, Kakitsuka T and Fujisawa T 2008 *IEEE J. Sel. Topics Quantum Electron.* **14** 992

[7] Sato T, Mitsuhara M and Kondo Y 2008 *The 2008 IEEE 20th Conference on Indium Phosphide and Related Materials* Versailles, France May 7–25, 2008 p. 1

[8] Tournié E, Grunberg P, Fouillant C, Baranov A, Joullié A and Ploog K H 1994 *Solid State Electron.* **37** 1311

[9] Mitsuhara M and Kondo Y 2007 *Electron. Lett.* **43** 1143

[10] Sato T, Mitsuhara M, Nunoya N, Kasaya K, Kano F, Takeshita T and Kondo Y 2007 *Proc. 20th Annual Meeting of IEEE Lasers and Electro-Optics Society* Piscataway, USA, October 21–25, 2007 p. 697

[11] Fujisawa T, Sato T, Mitsuhara M, Kakitsuka T, Yamanaka T, Kondo Y and Kano Y 2009 *IEEE J. Quantum Electron.* **45** 1183

[12] Lassen B, Lew Yan Voon L C, Willatzen M and Melnik R 2004 *Solid State Commun* **132** 141

[13] Veprek R G, Steiger S and Witzigmann B 2008 *J. Comput. Electron.* **7** 521

[14] Gu Y X, Yang T, Ji H M, Xu P F and Wang Z G 2010 *Chin. Phys.* B **19** 088102

[15] Schliwa A 2007 *Electronic Properties of Self-organized Quantum Dots* Ph.D. Thesis (Berlin: The Technical University of Berlin)

[16] Stier O 2000 *Electronic and Optical Properties of Quantum Dots and Wires* (Berlin: Wissenschaft and Technik Verlag)

[17] Foreman B A 1997 *Phys. Rev.* B **56** R12748

[18] Burt M G 1992 *J. Phys.: Condens. Matter* **4** 6651

[19] Vurgaftman I, Meyer J R and Ram-Mohan L R 2001 *J. Appl. Phys.* **89** 5815

[20] Chuang S L 1991 *Phys. Rev.* B **43** 9658

[21] Ke S H, Wang R Z and Huang M C 1993 *Acta Phys. Sin.* **42** 1510 (in Chinese)

[22] Veprek R G, Steiger S and Witzigmann B 2007 *Phys. Rev. B* **76** 165320

[23] Tompsett M F 1972 *J. Vac. Sci. Technol.* **9** 166

[24] Fang Z M , Ma K Y, Jaw D H, Cohen R M and Stringfellow G B 1990 *J. Appl. Phys.* **67** 7034

[25] Sato T, Kondo Y, Sekiguchi T and Suemasu T 2008 *Appl. Phys. Expr.* **1** 111202

[26] Matthews J E and Blakeslee A E 1974 *J. Cryst. Growth* **27** 118